Materials properties characterization in the most extreme environments

Daniel K. Schreiber, Ruth Schwaiger, Martin Heilmaier, and Scott J. McCormack*

There is an ever-increasing need for material systems to operate in the most extreme environments encountered in space exploration, energy production, and propulsion systems. To effectively design materials to reliably operate in extreme environments, we need an array of tools to both sustain lab-scale extreme conditions and then probe the materials properties across a variety of length and time scales. Within this article, we examine the state-of-the-art experimental systems for testing materials under extreme environments and highlight the limitations of these approaches. We focus on three areas: (1) extreme temperatures, (2) extreme mechanical testing, and (3) chemically hostile environments. Within these areas, we identify six opportunities for instrument and technique development that are poised to dramatically impact the further understanding and development of next-generation materials for extreme environments.

Introduction

Humankind has an innate appetite for exploration,[1–3] energy,[2–5] and speed[6] that requires materials to perform in the most extreme environments. While exploring the universe, systems can be exposed to extreme cold (~3 K in deep space), extreme heat (~1723 K reentry into Earth's atmosphere), harsh radiation (high-energy radiation and swift heavy ions), and tremendous strains (ballistic impacts from high-speed particles). Energy can be harnessed from the Sun on Earth through concentrated solar power,[5] where the Sun's rays are focused and stored as heat in molten salts at up to 973 K.[7] Next-generation nuclear fission reactors could pump corrosive molten salts as fuel and/or coolants at high temperatures to increase efficiency,[8] with designs reaching up to ~1773 K,[9] and nuclear fusion[4] technologies operate at even higher temperatures. Related nuclear thermal propulsion systems[2] require temperatures up to ~3100 K to thrust next-generation spacecrafts to Mars[3] and beyond. Even on Earth, hypersonic aircraft will experience leading-edge temperatures up to ~3000 K[6] (at Mach 8) that require materials to both resist oxidation and tolerate high stresses to prevent deformation midflight. These are just a few examples of the overarching need for next-generation materials to operate in the extreme environments required to propel civilization into the future.

Effective design of material systems to operate in extreme environments requires a clear understanding of the following: (1) their thermodynamics and fundamental properties, (2) their kinetics and transport properties, and (3) their evolving microstructure on multiple length and time scales. Traditionally, materials design has relied on trial-and-error Edisonian approaches and only more recently have computational tools been significantly leveraged to drive material development. Integrated computational materials engineering (ICME) approaches have proved fruitful in the past for designing innovative material systems on demand. The ferrium C64 steel[10] was predominantly designed through computational methods for rotorcraft drive trains in helicopters, and the ferrium M54 steel[11] was similarly designed for landing gears in aircraft. To do so, these steels, their composition, and manufacturing parameters were predominately predetermined via computational methods to meet the specific needs of their application. So why can't we design material systems for the extreme conditions of hypersonic platforms or nuclear fusion using similar on-demand methodologies today? Underpinning the successes

Daniel K. Schreiber, Pacific Northwest National Laboratory, Nuclear Sciences Division, Richland, USA; daniel.schreiber@pnnl.gov
Ruth Schwaiger, Institute of Energy and Climate Research, Forschungszentrum Jülich, Jülich, Germany; r.schwaiger@fz-juelich.de
Martin Heilmaier, Institute for Applied Materials, Karlsruhe Institute of Technology, Karlsruhe, Germany; martin.heilmaier@kit.edu
Scott J. McCormack, Department of Materials Science and Engineering, University of California, Davis, Davis, USA; sjmccormack@ucdavis.edu
*Corresponding author
doi:10.1557/s43577-022-00441-z

of these previous ventures were fundamental insights derived from years of experimentation and the subsequent construction of self-consistent materials properties databases. Comparable databases have yet to be derived for materials under more extreme conditions, especially under combined extreme conditions. In this article, we describe the current state-of-the-art experimental capabilities for testing materials under extreme environments and highlight the limitations of these approaches. Although there are many different "extremes" that fit this general description, we focus on three key areas that are relatively ubiquitous to challenge material performance: (1) extreme temperatures, (2) extreme mechanical testing, and (3) chemically hostile environments. Our aim is to identify capability gaps that if filled will enable the collection of all important materials data to facilitate the design of next-generation materials that will survive the most extreme environments.

Materials at extreme temperatures

Extreme temperatures are defined here as above 2000 K and below 77 K. Levitation in conjunction with laser heating can achieve extremely high temperatures (~4000 K) and be coupled with materials diagnostics to extract key thermochemical and thermophysical properties. Complementary to this, high-temperature imaging and thermal properties can be extracted from microscopy and calorimetry at more modest temperatures (~1600–2873 K). By contrast, cryogenic experiments slow atoms down and can be coupled with microscopy and other imaging techniques to extract fundamental mechanisms related to physical phenomena.

Levitation in conjunction with laser heating (up to ~4000 K)

Levitation in conjunction with laser heating has become the go-to approach for the highest of temperature measurements. These container-less techniques are ideal as they prevent unwanted reactions with their surroundings. Multiple levitation methods can be selected depending on the material system, including electromagnetic levitation (EML),[12,13] electrostatic levitation (ESL),[14–18] and aerodynamic levitator (ADL),[19–21] which uses a conical nozzle levitator[22] (CNL) (**Figure 1**a), and acoustic levitator (AL)[23–26] (Figure 1g). The main lasers used for heating include (1) a CO_2 laser (10.6 μm), optimized for heating oxide-based materials; and (2) a Yb laser (1.07 μm), YAG (1.064 μm), and/or diode lasers (0.980 μm) optimized for heating metallic-based materials. EML can take advantage of inductive heating for metallic materials. The highest reported temperature is approximately ~3773 K,[27] with unpublished communications of ~4000 K being achieved on a molten HfO_2 with diameter ~2.5 mm using dual laser heating. In all cases, the best samples for levitation are ~2–3-mm-diameter spheroids. Ceramic solid oblated spheroids at 3200 K can have temperature gradients up to ~500 K/mm (depending on processing), which can be reduced to ~15 K/mm if the sample is a perfect sphere that spins on all axes. When molten, this temperature gradient can be reduced to ~5 K/mm through convection.[28]

These levitation systems equipped with laser heating have been coupled with a variety of techniques to probe various materials properties, such as (1) *in-situ* high-speed pyrometry for melting point measurements (thermochemical); (2) drop-and-catch calorimetry for enthalpy measurements (thermochemical; (3) *in-situ* high-speed cameras for density, surface tension, and viscosity experiments (thermophysical); and (4) *in-situ* x-ray and neutron diffraction for local structure (short-range order), crystallography (long-range order), and phase diagram determination (multiphase order).

In-situ high-speed pyrometry is probably the simplest high-temperature diagnostic technique. It involves observing a sample with a high-speed pyrometer that monitors the surface temperature. The key challenges with these experiments are as follows: (1) ensuring the sample's levitation is stable, (2) ensuring the sample's temperature gradient is minimized, and (3) knowing the emissivity of the sample so that the temperature can be accurately determined. An EML has been used to measure high-temperature spectral emissivity when equipped with a spectrometer, but this system is highly custom.[29] High-speed pyrometry is best known for its recalescence experiments. For pure materials, the melting point can easily be extracted (Figure 1b). For multicomponent systems, liquidus and solidus temperatures can be extracted, but is more difficult and requires more statistics. Liquidus temperatures in oxide systems that have been examined include HfO_2-Ta_2O_5 (up to 3200 K),[30,31] $(Fe,Cr,Al)_3O_4$ spinels with variation in oxygen partial pressure (up to 2000 K),[32] and others.[33,34]

Drop-and-catch calorimetry utilizes ADL via a CNL with a split nozzle and laser heating to achieve temperatures up to 3700 K. Once the sample has equilibrated, the split nozzle is opened, allowing the high-temperature sample to fall and be caught between two copper heat sinks maintained at 298 K that are attached in series to two semiconductor heat flux transducers (Figure 1d–e). By heating samples above and below their melting points, enthalpies of fusion can be measured (Figure 1f). This design has advantages over conventional drop calorimetry in which a sample is heated in a furnace and dropped into a calorimeter at ambient conditions (e.g., UO_2,[35] SiO_2[36]). These older designs required large samples (10–100 g) encapsulated in metallic containers where the sample can potentially react with the container leading to erroneous results. The drop-and-catch system combined with ADL overcomes this key limitation and allows for higher temperature enthalpy of fusion measurements (e.g., Al_2O_3,[37] Yb_2O_3,[38] Lu_2O_3,[38] ZrO_2,[39] and HfO_2[39]). A key need for this technology is to develop a drop-and-catch calorimeter where the environment can be controlled, allowing for enthalpy of fusion measurements on air-sensitive intermetallic compounds and refractories such as carbides, nitrides, and diborides.

High-speed cameras can be used in conjunction with high-temperature levitation to measure many physical phenomena in the melt and upon solidification as function of temperature (Figure 1h). Image processing utilizing machine learning algorithms

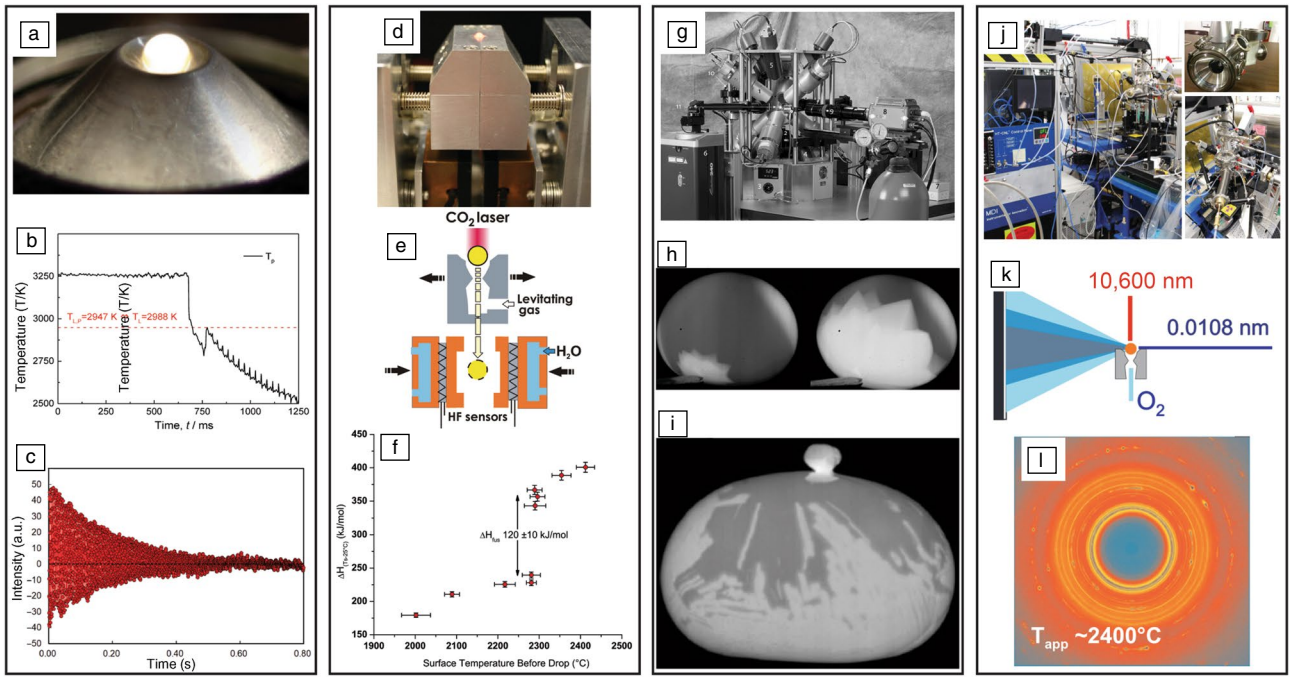

Figure 1. Levitation with laser heating techniques coupled with materials diagnostic. (a) Optical image of a conical nozzle levitator (CNL) developed by Materials Development, Inc.[22] levitating a spherical sample. (b) Cooling trace of ZrO_2 showing a recalescence peak.[47] (c) Oscillation decay of molten Co-Cr-Mol melt at 1873 K used to determine viscosity and surface tension collected on electrostatic levitation.[50] (d) Optical image drop-and-catch calorimeter.[37] (e) Schematic of a drop-and-catch calorimeter.[37] (f) Enthalpy measurements collected using a drop-and-catch calorimeter showing the enthalpy of fusion for Al_2O_3.[37] (g) Acoustic levitator.[24] (h) Partially crystallized undercooled $Y_3Al_5O_{12}$ at ~1473 K. Crystallization was initiated by a stinger.[24] (i) Solid Y_2O_3 undergoing hexagonal to cubic phase transition at 2599 K.[24] (j) CNL setup at Argonne National Laboratories Advanced Photon Source for *in-situ* high-temperature x-ray diffraction.[27] (k) Schematic of the CNL coupled with *in-situ* x-ray diffraction.[85] (l) *In-situ* x-ray diffraction of Y_2O_3 at ~2773 K.[85]. HF heat flux. Each image in this panel was reproduced with permission from its respective journal.[22,24,27,37,47,50,85]

for sample edge detection is implemented enabling *in-situ* volume calculations,[40] and in turn, density measurements.[19] This has been implemented to measure densities of various metallic melts (e.g., Si,[41–43] Mo,[44] Ta,[44] Re,[45] and Os[45]) via EML and ESL above 3500 K and oxide melts (e.g., Al_2O_3,[19] Y_2O_3,[46] ZrO_2,[47] and HfO_2[46]) via ADL and AL above 3000 K. Viscosity[25] and surface tension[26] measurements can also be made by perturbing the melt with a mechanical pulse, causing the molten liquid to oscillate (Figure 1c). The oscillation damping time and resonance frequency are directly related to the viscosity and surface tension. Drop oscillation can only be used for low viscosity liquid droplets that can oscillate and thus can only measure viscosities similar to that of water, and struggle when melt viscosities are high. This technique has been used to measure viscosities and surface tensions of a variety of metallic systems (e.g., Ti,[48] Mo,[49] Pt,[48] and Co–Cr–Mo[50]) above 3500 K and oxide systems (e.g., Al_2O_3,[51] ZrO_2,[47] and SiO_2–CaO–Al_2O_3 slags[52]) above 3000 K. Other interesting features that have been observed using these techniques include *in-situ* identification of invariant reactions, such as the monotectic in ZrO_2–SiO_2[53] system and the hexagonal to cubic transition in Y_2O_3 at ~2599 K (Figure 1i).

X-ray and neutron diffraction have been coupled with levitation and laser heating internationally at multiple synchrotron (Figure 1j–l) and neutron sources. Traditionally, these systems were used to examine the local structure of high-temperature melts. For example, the local structure of molten $(Y_2O_3)_x(Al_2O_3)_{1-x}$ up to 2770 K was examined using ADL with laser heating.[54] This analysis revealed that the Y–O and Y–Y coordinations in Y_2O_3 were the same in high-temperature hexagonal polymorphs as they were in the melt. In contrast, the addition of Al_2O_3 greatly altered the local structure. These findings are significant as these local structures demonstrate a change in entropy on melting that greatly informs our understanding of the melting point and process. Similar studies have applied this method to many other high-temperature molten oxide systems (e.g., Al_2O_3, UO_2,[55] and UO_2-ZrO_2[56]).

Crystallographic information can also be extracted from solids at high temperatures. The change in tetragonality of HfO_2 approaching the tetragonal to cubic transition at ~2723 K was measured.[57] Critical transitions for next-generation barrier coatings[58] have been discovered and studied, such as the peritectic transition in $Hf_6Ta_2O_{17}$[59,60] that occurs at ~2523 K. The anisotropic thermal expansion of a series of oxides has been measured from room temperature (RT) up to complete melting (e.g., YSZ[61] (Figure 1l), $La_2Zr_2O_7$,[61] $Hf_6Ta_2O_{17}$,[59] and $HfTiO_4$[62]), which are critical for the design of next-generation

high-temperature barrier coatings. Furthermore, entire phase diagrams have been investigated and built *in-situ* using this high-temperature levitation technique, such as the HfO_2-Ta_2O_5 system up to 3200 K.[30,31]

There are additional examples in the literature where high-temperature levitation is coupled with other x-ray, neutron, and nuclear magnetic resonance (NMR) techniques. These include (1) x-ray absorption spectroscopy (XAS) for element-specific local structure,[63,64] (2) small-angle x-ray scattering (SAXS) for liquid–liquid phase transitions,[65,66] (3) inelastic x-ray scattering (IXS) for local structure dynamics and local viscosity measurements,[67–69] (4) small-angle neutron scattering (SANS) for phase separation,[70] (5) quasi-elastic neutron scattering (QENS) for liquid diffusion coefficient measurements,[71,72] and (6) NMR for *in-situ* local structure coordination measurements.[73–77]

High-temperature imaging and thermal properties (up to ~3273 K)

Beyond levitation and laser heating, many other important high-temperature characterization techniques can operate above 1500 K. The discussion gives some noteworthy examples of (1) high-temperature microscopy and (2) calorimetry.

Conventional heating systems in a transmission electron microscope (TEM) are limited to ~1073 K due to the temperature limitation of the surrounding materials in the microscope. Specialized systems that take advantage of laser pulses enabling highly localized heating can achieve temperatures up to 2273 K.[78] These pulses also provide a unique avenue to observe dynamic phenomena in pump-probe setups. For example, the dynamic transmission electron microscope (DTEM) and its more recent variants[79] can provide snapshots of phase changes and melt solidification fronts.[80–82] One interesting recent development is the use of electron energy gain/loss spectroscopy to measure the sample temperature of a boron nitride via spectrum shifts from RT to 1600 K at the nanoscale.[83] Although these measurements require highly specialized scanning transmission electron microscopes (STEMs) with exceptional electron energy resolution, the approach highlights as-yet untapped opportunities for extreme temperature studies of materials behavior with (sub)nanoscale spatial resolutions unapproachable by beamline or other "bulk" methods.

Differential thermal analysis (DTA) can reach temperatures upwards of 2873 K.[84,85] In DTA, the temperature difference between the sample and a reference is recorded on heating and cooling. Classical DTA geometries allow fast response times, but are unable to quantitatively measure heats of reaction, as the magnitude of the thermal arrest is dependent on sample heat capacity and thermal conductivity.[86] In the Boersma DTA[87,88] design, metallic crucibles are used and temperature differences between sample and reference are measured, allowing for calibration and accurate measurements of thermal arrest. The temperature range of a DTA is limited by the thermocouple material. In air, this is approximately 1873 K when using a S-type or B-type thermocouple. In a vacuum or graphite furnace, 2673 K may be reached using WRe thermocouples. The highest temperature DTA constructed reached 2873 K with a WRe20-W thermocouple.[84] When using DTAs at these higher temperatures, samples should be sealed in W containers to prevent carbon contamination.[89]

High-temperature oxide melt solution calorimetry[90] is an advanced calorimetry technique that uses high-temperature oxide solvents to dissolve refractory materials to measure their enthalpy of dissolution. By carefully defining a dissolution thermal cycle, the enthalpy of formation of a compound,[91,92] the enthalpy of mixing[93–95] of a solid solution, and even surface enthalpies[96–99] can be accurately measured. The main solvents used in the process include lead borate ($2PbO{\cdot}B_2O_3$)[100] and sodium molybdate ($3Na_2O{\cdot}4MoO_3$).[101,102] This technique has been used predominantly on oxides.[90] More recently, molten sodium molybdate (at 973–1073 K) has shown to be an excellent catalyst for the rapid oxidation and dissolution of other ceramics such as nitrides[103–105] and carbon-based materials (polymer-derived ceramics),[106,107] but more work is required for the complete dissolution of diborides. These formation, mixing, and surface enthalpies are critical for thermodynamic assessments of high-temperature refractory systems to understand their stability under a variety of conditions that are essential to the success of ICME approaches.

Cryogenics (down to ~1.8 K)

At the other end of the temperature spectrum, cryogenic temperatures challenge materials by freezing out atomic motion and structural relaxations. This leads to the classical structural ductile-to-brittle transition in many alloys[108] and functionality changes, including superconductivity and magnetic phase transitions.[109] The specific temperatures and properties of interest are quite diverse, and here, we limit the discussion to high-resolution cryogenic characterization techniques that are relatively agnostic to the specifics of the underlying materials science problem. These include (1) low-temperature physical property measurement system (PPMS),[110–112] (2) cryogenic electron microscopy (cryo-EM),[113] and (3) atom probe tomography (APT).[114,115]

PPMS from Quantum Design can be used to reliably measure the heat capacity of powders down to 1.8 K.[110,116] If the powders are thermally insulative, such as oxides, a copper sample container and copper strips can be used to enhance heat transfer[111] and improve accuracy. Powders can also be sealed under pressure up to ~700 kPa.[112] The low-temperature PPMSs are essential for magnetic measurements and standard molar entropy measurements from low-temperature heat capacity. With the increased interest in multicomponent alloys, particularly in high-entropy alloys (HEAs), and entropy stabilized materials,[117–119] the standard molar entropy (related to the entropy of formation) becomes essential in determining if the material is entropy stabilized with respect to its components.

In comparison with ultrahigh-temperature high-resolution microscopy, cryo-EM is clearly more mature. Cryo-EM development was driven heavily by the life sciences, where cryogenic vitrification was necessary to preserve cells and

other soft materials for high-resolution TEM observation or diffraction[120,121]—an achievement recently recognized by a Nobel Prize.[122] Materials scientists have been slower to embrace the value of cryo-EM methods, with most applications involving the preservation of materials that are otherwise unstable in conventional imaging conditions.[113] These can range from electron–beam-sensitive materials (e.g., alkali-rich battery materials or glasses, hydrated materials),[123–125] or environmentally sensitive materials that would react or evolve at RT (e.g., catalysts, actinides, or naturally aging alloys).[126] Beyond sample preservation, cryo-EM methods provide unique opportunities to study low-temperature phase transitions, including magnetic and superconducting transitions relevant to quantum materials. Such opportunities have, as yet, been largely unexplored[127] with scanning probe or bulk methods being more prominent.

APT is oftentimes used as a complementary high-resolution technique to TEM by providing subnanometer resolution, 3D elemental atom maps of buried interfaces, such as grain boundaries or heterophase interfaces.[114,115] APT is natively a cryogenic technique, where the needle-shaped, nanoscale specimen is maintained at ~20–60 K to prevent surface diffusion. Materials scientists are beginning to explore the potential of cryo-preservation of specimens for APT analysis. Oftentimes these are for environmentally sensitive materials that would oxidize, form hydrides, or age in typical laboratory conditions, but also include preservations of water/solid interfaces during corrosion[128–130] and hydrogen (deuterium) distributions in steels susceptible to hydrogen embrittlement.[131,132] Unfortunately, the technique does not lend itself well to high-temperature extremes (although in principle heating is feasible with the *in-situ* laser of most APTs).[133] However, quasi *in-situ* material aging or oxidation experiments are possible with inline reactors attached to the ultrahigh vacuum (UHV) buffer of the APT.[134,135] These are currently limited to ~1073 K, but could be extended to more extreme temperatures in a similar way as TEM methods via localized laser heating.

Although most cryogenic microscopy methods are aimed at preserving a material from damage or change during imaging, a significant opportunity exists to further exploit these techniques for functional materials to directly probe materials properties, and changes in properties, under cryogenic *operando* conditions. Certainly, work is ongoing in this area, particularly for magnetic imaging,[136] but with growing interest in quantum materials, significant opportunity exists to expand and leverage *in-situ* cryogenic microscopy methods. Beyond static imaging, these can include applied electrical or magnetic fields, or even irradiation, to drive ferromagnetic and ferroelectric domain walls,[109] electrical transport behavior,[137] or structural phase transformations.[138]

Extreme mechanical testing

Mechanical testing is inherently challenging due to required material geometries that ensure specific stress and strain states. The stochastic nature of brittle materials provides a further challenge where large statistics are required to describe the distribution of material failure states. These challenges are compounded when moving to testing extremes. Here, we group the discussion on extreme mechanical testing as (1) mechanical testing at extreme temperature performed in conjunction with a variety of materials diagnostic techniques, (2) small-scale mechanical testing and its benefits, and (3) *in-situ* microscopy mechanical testing.

Mechanical testing at extreme temperature

The success of mechanical testing at ultrahigh and ultralow temperature depends not only on controlling the test temperature, but mitigating other extraneous factors within the test system itself, the gripping system, the specimen design, and even the underlying strain measurements. These challenges have, to date, limited the maximum test temperature for commercial mechanical testing systems to ~1800 K, which is less than many service temperatures, such as ~2273 K for hypersonic platforms.

To investigate materials at 2273 K and higher, customized systems have been designed facilitating mechanical behavior studies of ultrahigh-temperature ceramics (UHTCs) and refractory alloys using ohmic heating of conducting samples and pyrometer-based temperature control.[139,140] Tensile tests of tungsten sheet (1-mm thickness) have shown the tensile strength and yield strength decreased from ~105 MPa and ~62 MPa, respectively, at 2073 K, to ~21 MPa and ~16 MPa, respectively, at 2773 K[140] (**Figure 2**a). To ensure temperature homogeneity over the test volume, the samples had a gage length of 10 mm, and noncontact strain measurement used machined shoulders as markers (Figure 2a). High-temperature testing can also be achieved by induction heating, which is suitable for both conductive and nonconductive materials. Induction heating of a graphite hot zone in an environmental chamber (Figure 2b) was used to conduct four-point bending tests of various zirconium-diboride-based UHTCs up to 2573 K.[141–144] These revealed that the flexure strength of pure ZrB_2 of ~200 MPa (1673–2573 K, in Ar)[141] was increased in ZrB_2-10 vol% ZrC ceramic up to ~460 MPa at 1673 K and ~360 MPa at 2573 K.[142] The temperature limit in these flexure strength experiments is related to the sample forming a eutectic with the graphite grips. More recently, the four-point flexural strength of single-phase high-entropy carbide ceramics was reported (Figure 2c) as ~90 MPa at 2573 K compared to ~420 MPa at RT.[143] An electric resistance furnace also enabled high-temperature tensile testing ZrB_2–20 vol% SiC in air up to 1973 K.[145] Ductile fracture behavior and ~0.5% plastic strain was observed at 1973 K in an oxidative environment.

Ideally, noncontact methods are used to ensure accurate and reliable strain measurement at ultrahigh temperatures as strain gauges and clip-on extensometers are limited to lower temperatures and larger samples. At ultrahigh temperatures, even small contact forces may lead to critical stress concentrations and premature failure, especially in small specimen sizes. Recently, an ultrahigh-temperature video extensometer

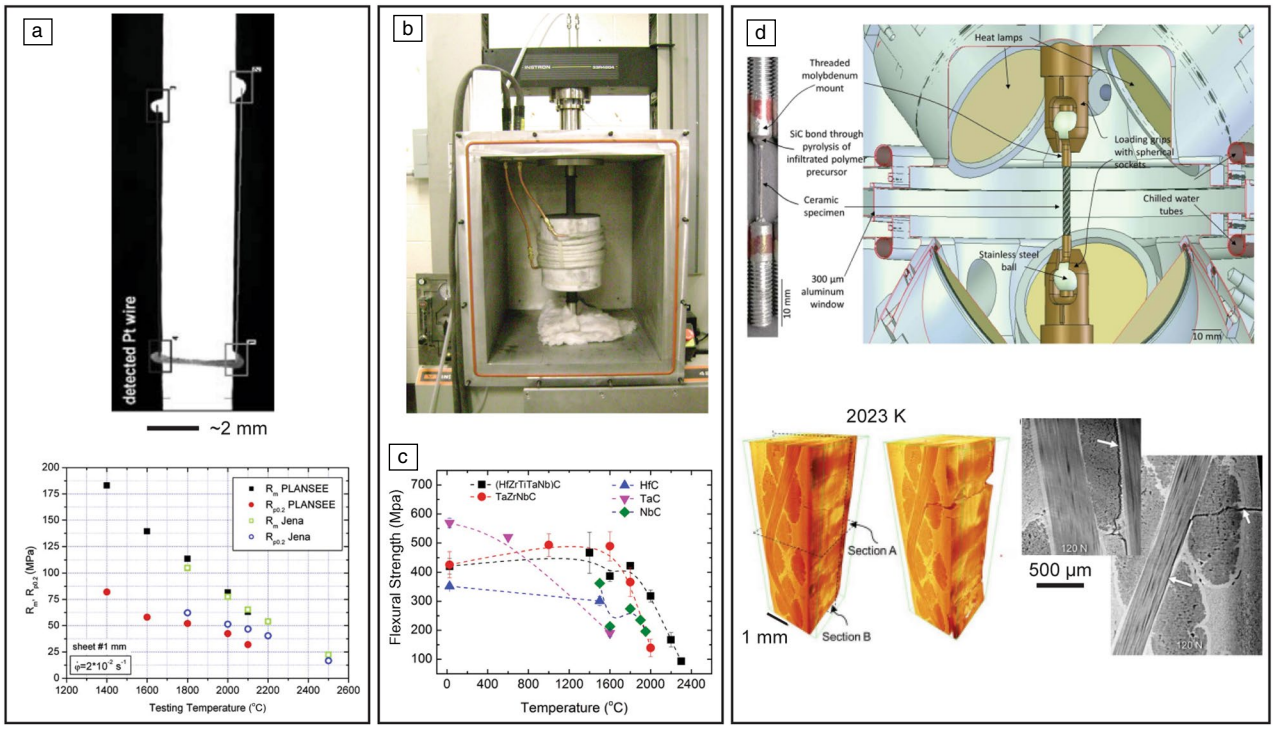

Figure 2. Mechanical testing at temperatures >2000 K requires customized setups and adjusted sample geometries to facilitate reliable strain measurement and stable temperature control. (a) Markers machined into the sample, such as shoulders or wires wrapped around the sample, enable noncontact strain measurements.[140] Tensile tests of tungsten conducted with this geometry allowed the characterization of the mechanical properties up to temperatures of 2773 K.[140] (b) High-temperature testing accomplished by induction heating of a graphite hot zone in an environmental chamber[144] is used for four-point bending tests of ultrahigh-temperature ceramics up to 2573 K. This figure has been reproduced with permission of The American Ceramic Society. (c) The strength of single-phase high-entropy carbide ceramics was determined up to a temperature of 2573 K. The flexural strength stayed above ~400 MPa up to 2073 K, then decreased nearly linearly to ~90 MPa at 2573 K.[143] (d) Test specimen and schematic showing a test specimen being mounted in the rig at the Advanced Light Source. Below is a 3D *in-situ* tomography of C–SiC composite under a tensile load at 2023 K.[147] Each image in this panel was reproduced with permission from its respective journal.[140,143,144,147]

for real-time high-temperature strain measurement, based on speckle patterns enabling 2D spatially resolved strain, was presented and validated by uniaxial tests of tungsten-molybdenum alloys.[146] At 2273 K, debonding of the speckle pattern was observed, hampering its operation at higher temperatures. Instead, markers can be machined (Figure 2a) in the sample, such as shoulders with well-defined contours[139] or thin wires wrapped around the specimen,[140] and were used successfully for strain measurements with a maximum error of ±0.07 percent. Although useful, 2D strain cannot be resolved spatially.

An *in-situ* test rig for mechanical loading at temperatures up to 2273 K in controlled environments (i.e., under vacuum or a controlled gas flow) in combination with x-ray microtomography (µCT) was designed and fabricated for use at the Advanced Light Source (ALS) at Lawrence Berkeley National Laboratory (LBNL).[147,148] The high x-ray flux characteristic of synchrotron sources in conjunction with high resolution detectors enables high-resolution µCT data sets with resolution of 600 nm/pixel to be acquired within 100 s or even faster. The time resolution is much faster when compared to lab-based instruments allowing the direct observation of microstructural changes during mechanical testing at high temperatures. In the ALS setup (Figure 2d), heating is achieved by six radiant lamps with elliptical reflectors that focus at a point, achieving a ~5-mm-diameter hot zone on the sample. Chamber and loading system are water-cooled to ensure thermal stability. Tension, compression, and bending loads can be applied, allowing the determination of mechanical properties at extremely high temperatures and unprecedented insights into materials deformation and failure behaviors,[148] such as crack growth in carbon fiber-reinforced ceramic matrix composites (Figure 2d).

Determination of the mechanical properties of materials under the combined effects of high temperature and high strain rates represents another challenge. In bulk samples, high strain rate testing is typically accomplished using a split Hopkinson bar apparatus reaching strain rates from 10^2 to 10^5 s^{-1}.[149] Various heating methods have been designed for high-temperature split Hopkinson bar tests.[150] The most common approach of simply heating the specimen in contact with the incident and transmission bars results in a large temperature gradient and potentially microstructural changes in the elastic bars. Preheating the specimen and keeping the elastic bars away from the

hot zone helps to reduce temperature gradients and increase the specimen temperatures.[151]

Designing materials for extreme environments also relates to low and cryogenic temperatures. For tensile, fracture, and fatigue testing at cryogenic temperatures, the specimens are typically immersed in a coolant such as liquid helium (4.2 K) or liquid nitrogen (77 K) to reach and maintain the low test temperature against heat generated by the mechanical loading. The mechanical properties of face-centered-cubic (fcc) metals such as austenitic stainless steels, aluminum alloys, copper alloys, and the hexagonal close-packed (hcp) titanium alloys have been studied extensively, as they are most frequently used at cryogenic temperatures.[152] HEAs have drawn additional interest for cryogenic applications[153] and the single-phase equimolar fcc alloy CoCrFeMnNi has been the most widely studied. CoCrFeMnNi exhibits an excellent strength-ductility combination,[154] different from the ductile–brittle transition of the traditional alloys. The tensile strength and strain reached at 4.2 K were ~1.2 GPa and >60%, respectively.

Small-scale mechanical testing

Small-scale mechanical testing under extreme conditions is gaining popularity as only small amounts of materials are needed, and thus mechanical property changes can be evaluated efficiently. Furthermore, small-scale testing methods also enable targeting specific microstructural features or areas on the sample surface of interest.

Nanoindentation testing is one of the most popular techniques for mechanical characterization at ambient temperatures and has also become popular for high-temperature testing.[155,156] The simple sample geometry needed for nanoindentation is advantageous compared to standard tension and compression samples, which need larger quantities of materials and more elaborate fabrication. Nanoindentation at temperatures up to 700 K is used routinely to determine deformation mechanisms and thermal activation parameters for metals and alloys,[157,158] and recently nanoindentation experiments at 1373 K[159] were demonstrated. Identifying the most suitable tip material is probably the biggest challenge, because chemical reactions or tip wear need to be avoided during the indentation process. Tungsten carbide was identified as the material with the lowest chemical reactivity with the largest number of elements.[160]

The low-temperature regime is relatively unexplored with respect to nanoindentation. Similar to macroscopic tensile tests, materials and indenter tips can be immersed in cryogenic liquids to ensure constant temperature when contact is made. Typically, such methods do not allow for measuring the indentation depth but analyze the size of the impression, as done in macroscopic hardness testing. Peltier coolers can also be attached to the sample and the indenter tip[161] and have allowed measuring the displacement at a reasonable thermal drift rate, but because the setup was operated in air, ice crystals formed on the sample surface for temperatures <273 K. This problem can be solved by operating in vacuum, shown more recently for a depth-sensing indenter system[162] where a cold finger design allowed temperatures down to 150 K.

For irradiated materials, small-scale mechanical testing is also popular[163,164] because the material's properties can be evaluated from small volumes of (expensive and radioactive) reactor-irradiated materials or from the (relatively cheap and typically not radioactive) thin surface layers of ion-beam irradiated samples. Small neutron-irradiated materials are not considered radioactive by many laboratory radiation safety metrics because of the small radioactive volumes. Nanoindentation methods have also been the most popular small-scale testing technique used in combination with electrochemical hydrogen charging to study the effects of hydrogen on the mechanical properties of materials[165–168] elucidating the mechanisms of hydrogen embrittlement.

On the other hand, small-scale high strain-rate testing is still in its infancy. Small-scale mechanical testing is typically conducted at strain rates between 10^{-5} and 10^{-2} s^{-1}, whereas macroscale devices like the split Hopkinson bar can reach strain rates several magnitudes higher. Although some nanoindentation instruments are already capable of high strain-rate testing reaching 1000 s^{-1},[169,170] these methods are not yet routinely used for measuring fundamental mechanical properties at high strain rates.

High-resolution characterization of deformed microstructures

High-resolution microstructural characterization complements mechanical testing with atomic-to-mesoscale observations of material deformation. TEM plays a vital role here with broad analytical flexibility to describe both structural and microchemical material changes across length scales. Classic examples include dislocation imaging,[171] analyses of evolving grain-boundary structures and chemistry, local strain mapping, and crack-tip analyses.[172] Most often these analyses are performed *ex situ* (i.e., postmortem) after mechanical testing, providing a static snapshot of the final, and often structurally failed, microstructure. The analytical methods include electron diffraction (atomic order and structural defects in a material), energy-dispersive x-ray spectroscopy (EDS—elemental composition), and electron energy-loss spectroscopy (EELS—elemental composition and chemical bonding information). Four-dimensional-STEM, which involves collecting local diffraction patterns at each pixel during a nanoscale electron probe scan, is a relatively new and promising method[173] for nanoscale strain maps (e.g., around crack tips) and the interplay of local ordering and material deformation. *In-situ* TEM mechanical testing has made tremendous strides in recent years, especially in nanopillar compression, tension, or cantilever testing, and extending to tribology and shear[174,175] to provide more direct connections between high-resolution observation and mechanical response. These nanoscale samples are most often prepared by focused ion beam (FIB) milling with a Ga+ ion beam, which has potential negative effects on the resulting mechanical behavior that should be considered.[176]

At the same time, the rate at which data are being generated, both with *in-situ* and *ex-situ* analyses, presents a challenge for materials scientists and data scientists alike.[177] This trend will continue as *in-situ* experiments continue to push the boundaries of what is possible and generate data faster than the scientist can analyze it.

Material degradation in chemically hostile environments

Most materials are natively far from thermodynamic equilibrium in their typical use environment and can be even more so in certain extreme environments. Chemical reactions between the material and environment drive deleterious microstructural evolution. At elevated temperatures, materials are required that can withstand oxidative and other corrosive environments often over the course of long lifetimes. Although materials are engineered to tolerate or resist these changes, oftentimes by depositing or natively forming barrier layers separating the material and environment, increasingly hostile environments challenge our scientific and engineering capacities. Exemplary areas, which will be tackled in this section from the viewpoint of how to reliably measure material degradation, will be (1) molten salt corrosion with an emphasis on the applications in concentrated solar power (CSP) plants; (2) gaseous corrosion with an emphasis on space missions, including hypersonic flight with reentry vehicles and venus atmospheric corrosion; and (3) chemical implications at low temperature. The current state of testing for these three application scenarios is presented, which need seemingly different approaches with respect to temperature and atmosphere testing regimes.

Molten salt corrosion

Heat-transfer fluids (HTFs) and thermal energy storage (TES) materials must fulfill specific requirements, including high thermal conductivity and heat capacity, low viscosity, low melting, and high boiling points, alongside easy availability and limited environmental impact.[178–181] Currently, molten nitrate salts are employed as HTFs and for TES, but their thermal stability limits operation temperatures to about 838 K.[179,181,182] Because the energy-conversion efficiency of CSP systems increases with operating temperature, the next generation of CSP plants will operate at temperatures above 973 K.[180,183,184] On the one hand, this requires utilizing novel HTF and TES materials, such as molten eutectic chloride salts (e.g., NaCl-KCl-$MgCl_2$) that guarantee a low freezing point but high thermal stability at the same time.[183–185] On the other hand, long-term testing and sophisticated characterization techniques must be employed on the corrosion phenomena from these media.[185–187] An example for a state-of-the-art test setup is given in **Figure 3**a.[185] For the crucibles, high-temperature-resistant glassy carbon or alumina is usually used.[185,186] The experiments are carried out under flowing Ar atmosphere for times of up to 500 h and the temperature is controlled by PtRh10-Pt thermocouples within the molten salt. Although this experimental setup is capable of maintaining long-term testing and temperatures beyond those of actual CSP plants, there is still a lack of commercial structural alloys that can withstand those demanding conditions.[185–187] As an example, stainless steels 310 and 316, or Ni-base alloys such as Haynes 230, IN 600, or IN 625 suffer huge material losses ranging from 200 to 1700 µm/year along with extensive Cr leaching at 973 K that make them clearly unacceptable for these environments (Figure 3b).[185–189] Such behavior is perhaps ironic, as high-Cr alloys are commonplace in corrosion-resistant alloys in most oxide-forming environments where nanoscopic films of Cr_2O_3 protect the underlying alloy from further degradation. Similar responses have been observed in FLiNaK and FLiBe chemistries considered for molten salt cooled nuclear reactor designs, driving similar research efforts to identify and engineer new materials to withstand those related environments.[190–192]

Surprisingly, after the seminal work of Atmani and Rameau in 1980,[191,193] who investigated stress-corrosion cracking (SCC) of stainless steel in molten NaCl-$CaCl_2$ at 840 K utilizing a uniquely designed tensile test apparatus, few groups have aimed at studying the combined impact of mechanical stress and chemical attack under CSP conditions.[194] This research gap, in part, is a result of expected low-stress conditions of CSP or molten salt reactor designs, but localized attack and grain-boundary embrittlement could well be anticipated in service.[195] In research on T91 SCC,[194] tensile tests were carried out at low strain rates (around 10^{-6} s^{-1}) as calculated from the initial displacement rate in electromechanical test systems. For the corrosion chamber graphite crucibles or Ni-Cr-Mo alloys were employed, which makes direct strain measurement a challenge, if not impossible. Similarly, measurements of dynamic crack growth rates using electrical potential drop across the specimen[196] are quite difficult given the conductive nature of the salt media. As anticipated, the comparison with the material behavior at the same temperature, but in air, reveals substantial decays in both yield strength and ultimate tensile strength (UTS) as well as in obtainable ductility. Nevertheless, the scarce available information in the literature clearly demonstrates the detrimental impact of superimposed chemical attack on mechanical loading under CSP conditions.

Nanoscale characterization of atomic-level processes accompanying high-temperature salt corrosion are still limited in the literature. This is partially the result of difficulty in designing *in-situ* high-resolution salt corrosion experiments, and the air sensitivity of corroded surfaces, especially salt/alloy interfaces, for *ex-situ* examinations. Environmental control during *ex-situ* sample preparation is persistently vexing when studying the role of salt impurities on corrosion behavior, especially impurity oxidants, when laboratory air easily reacts with the salt at room temperature. Several opportunities exist for extending cryo-EM and cryo-APT methods to study (solidified) salt/alloy corrosion interfaces. In particular, methods developed for studying alkali-rich battery materials, which share many similar air-sensitivities with the salts here, could be leveraged.[125] High-resolution *in-situ* observations of salt corrosion fronts are also beginning to be possible. For example, high-resolution x-ray tomography measurements have

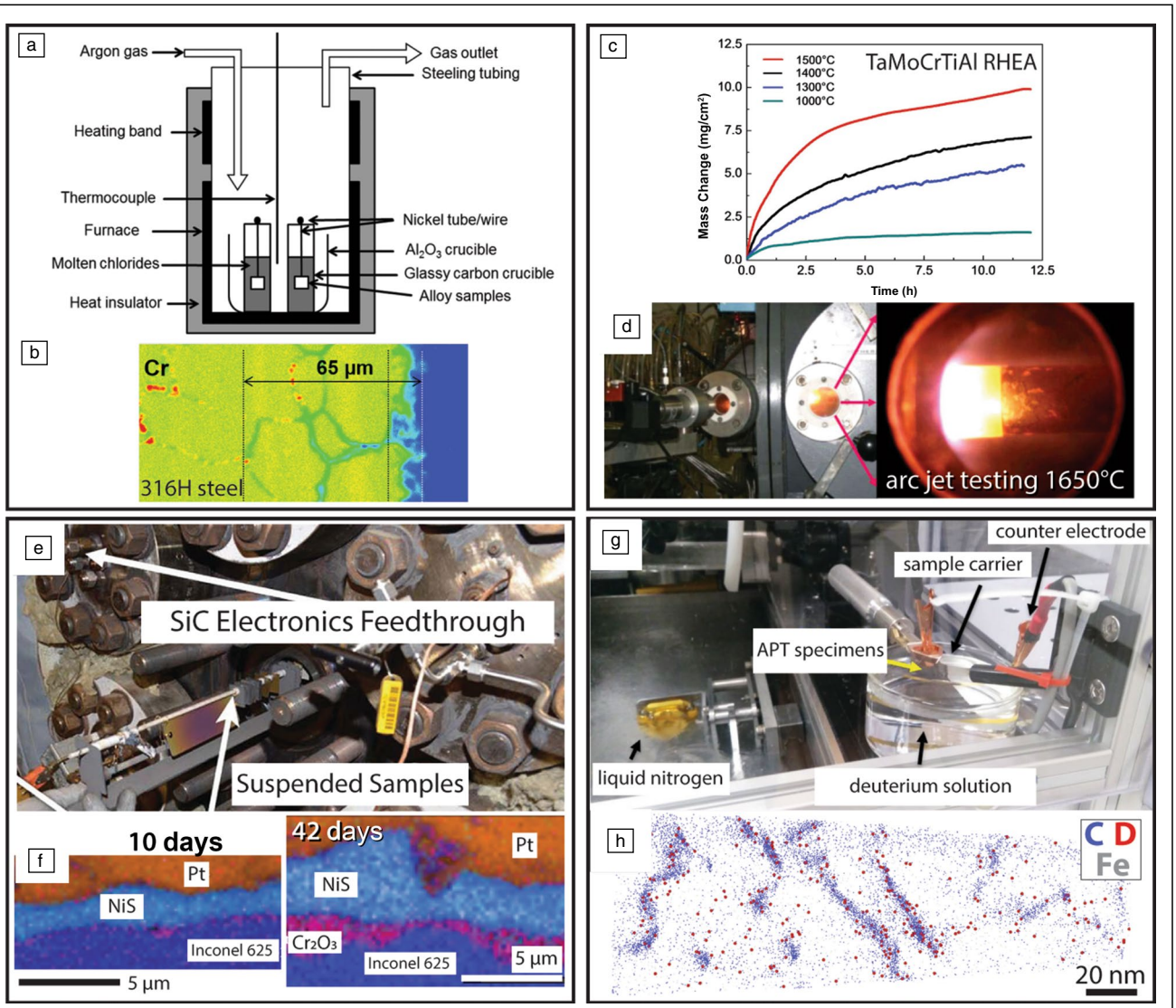

Figure 3. Experimental setups and analyses of materials exposed to (upper left) salt corrosion, (upper right) high-temperature gas, (lower left) highly corrosive gas, and (lower right) low-temperature hydrogen. Corrosive testing under extreme conditions. (a) A typical setup for molten salt corrosion testing at elevated temperatures with suspended coupon samples.[185] (b) Energy-dispersive x-ray spectroscopy (EDS) analysis of extensive Cr leaching from a 316H stainless steel after salt corrosion (NaCl-KCl-$MgCl_2$) at 973 K for 400 h.[189] (c) Continuous weight change curves of an equimolar Ta-Mo-Cr-Ti-Al RHEA in laboratory air between 1273 and 1773 K.[203] (d) Optical image of high-temperature arc jet testing of ultrahigh temperature ceramics at NASA HyMETS test facility.[209] (e) Optical image of sample loading into the GEER (Venus chamber)[219] and (f) EDS analysis of the resulting corrosion in Inconel 625.[219] (g) Experimental setup for deuterium charging of atom probe tomography (APT) specimens and cryogenic preservation[132] and (h) corresponding APT atom map of deuterium segregation to transgranular carbides on dislocations.[132] Each image in this panel was reproduced with permission from its respective journal.[132,185,189,203,219]

been made during salt corrosion of Ni-Cr alloys, which can exhibit a bicontinuous network of nanopores and Cr-depleted metal[197] similar to nanoporous Au formed from Ag-Au alloys.[198] Although aqueous corrosion has been studied via liquid-cell TEM,[199] similar inroads have yet to be made for molten salt corrosion with limited success having been found with iterative snapshots of salt corrosion on TEM samples.[200]

Gaseous corrosion

Research for high-temperature air and combustion environments focuses on increasing the temperature capability of material systems beyond those of existing Ni-based superalloys. Two primary material classes have been in focus for some years for applications in combustion engines, hypersonic flight, and reentry vehicles at temperatures up to 3273 K: UHTC based on borides, carbides, or nitrides[201–203] and refractory high-entropy alloys (RHEAs).[204] Oxidation testing at these extreme temperatures is usually done in (laboratory) air, either discontinuously in box/muffle furnaces with intermittent weight change measurements, or continuously by thermogravimetric analysis (TGA). Figure 3c displays such continuously measured weight changes of the equimolar

Ta-Mo-Cr-Ti-Al RHEA for a wide temperature range between 1273 and 1773 K. The moderate weight gains indicate good protectiveness of the complex $CrTaO_4$ scale at temperatures up to $\Delta T \approx 400$ K higher than those acceptable for state-of-the-art Ni-based superalloys.[205] To simulate reentry conditions, including thermal shock resistance, less expensive oxyacetylene torch tests[206–208] and more expensive arc jet tests in a temperature range between 1373 K (simulating hypersonic flights at Mach 6) and beyond 2273 K are carried out;[201–203] see Figure 3d representing a test of a ZrB_2/SiC-based composite, coated with Mo-Si-B, tested at NASA's HyMETS test facility.[209] However, as many of these materials are considered to form a protective silica scale, investigations under water vapor have additionally been carried out,[210,211] which clearly demonstrate (detrimental) accelerated scale growth under wet conditions. An interesting novel method for mechanical testing superimposed with wet air and sodium chloride (i.e., SCC) was exemplified recently for Ti alloys at elevated temperatures (723 K).[212] During two-point bend testing with a uniquely designed setup for 100 h, surprisingly little deuterium was taken up by the Ti alloy (<0.06 at.%), as determined by post-test APT analysis. By contrast, a significant impact on embrittlement was found from the severe oxygen pickup (>5 at.%) in the wake of the crack tip, eventually leading to the formation of alien phases.

High-resolution *in-situ* characterizations have yet to be established under comparable extremely aggressive conditions. State-of-the-art environmental TEM experiments are typically limited to ~1073–1273 K in flowing gas in either dedicated microscopes or cell-based sample holders.[213,214] However, these kinds of studies have still been informative for directly observing atomic-level dynamic phenomena otherwise only inferred. For example, oxidation of particles can reveal the evolution of a solid metal sphere to a hollow oxide sphere through Kirkendall effects of vacancy coalescence at the nanoparticle interior.[214] Currently, temperature limitations do affect the viability of this approach to *in-situ* ultrahigh-temperature oxidation studies. Although laser heating could extend the sample temperature to higher ranges, one must also consider the temperature of the surrounding gas and its flow rate and their impacts on the resulting behaviors. Lower-temperature *in-situ* oxidation or *ex-situ* characterization of previously oxidized samples is thus the current state of the art for nanoscale analyses. *Ex-situ* high-resolution TEM and APT are still likely to play a critical role in the ongoing development of corrosion-resistant materials, with nanoscale observations of the resulting chemical, structural, and elemental evolution, especially for compositionally complex RHEAs and their resulting oxides.[215,216]

The Glenn Extreme Environments Rig (GEER) can simulate many planetary environments include high temperature and high pressure along with multicomponent chemistry within a 0.914 m (3 ft.) diameter and 1.219 m (4 ft.) length.[217] Due to NASAs current interest in Venus,[218] GEER has been configured to mimic the Venusian atmosphere at the surface to about 75 km high. GEER can mimic the surface for more than 24 days with the following parameters: 773 K, 100 bar, CO_2-96.5%, SO_2-130 ppm, HF-5 ppm, HCl-0.5 ppm, NO-5.5 ppb, CO-15 ppm, COS-27 ppm, N_2-3.4%, and H_2O-30 ppm for 24 days.[217] Figure 3e shows samples being loaded into GEER. Several materials have been tested for survivability and durability, including electronics packaging materials (PbO, Al_2O_3), insulation (rock wool: CaO/SiO_2), SiC electronics (Au/Pt/Ir/Pt/TaSi2 bondpads, Au wires, Pt wires), feed-through materials (ceramawire), SiC pressure sensors,[219] and Inconel 625. Figure 3f shows a scanning electron microscopy EDS map of Inconel 625 degradation between 10 and 42 days in GEER, highlighting formation and growth of duplex corrosion layers. The large volume capacity of the system also allows for the testing of real systems. Several key systems have already been tested in GEER in preparation for a Venus mission including a SiC-based integrated circuit (IC) for electronic systems,[220,221] a high-temperature co-fired ceramic Al_2O_3 package with Au/Pt metallization system,[222] and a sensor system that measures the relative dielectric constant of gases within the Venus atmosphere.[223]

Chemical implications at low temperature

As one could expect, low temperatures are less associated with chemical material degradation than high temperatures as reactivity decreases. There is, however, one example worth highlighting: hydrogen embrittlement. Here, an alloy's ductility is significantly reduced due to the presence of hydrogen in the alloy, typically from environmental conditions. This embrittlement is exacerbated at low temperatures where hydrogen can enrich and trap at microstructural defects (precipitates, grain boundaries, or dislocations) to impede normal deformation mechanisms. Although these typically need not be cryogenic temperatures, direct observation of this predicted hydrogen trapping has only recently been made possible by advances in cryo-APT methods (Figure 3g), which complement integral methods of measuring hydrogen trap energies via thermal desorption analysis (TDA).[224,225] The challenge here is that very few analytical methods have sufficient spatial resolution and sensitivity to light elements (e.g., APT observation of a spiked deuterium isotope of hydrogen in Figure 3h). Furthermore, hydrogen is very mobile even at room temperature, so keeping hydrogen in a nanoscopic APT specimen is also nontrivial. With these advances in cryogenic sample preparation and handling, recent cryo-APT research is making great strides in revealing the atomic-level detail of hydrogen trapping underpinning embrittlement.[132,212,226,227] However, these studies have been limited to electrochemical hydrogen loading of samples and have yet to directly connect with mechanical testing of the hydrogen-loaded samples.

Overview and next steps

We have come a long way in the investigation of materials in the most extreme environments, ranging from temperatures as low as 1.8 K to as high as ~4000 K, including high stresses and strains coupled with temperature all the way to hot, corrosive,

and oxidative environments. These measurements will be critical to developing materials databases for predictive design of novel materials for these conditions, but much work has yet to be done and to push our testing limits even further. From this review, we have identified several key instrument and testing developments that can be pursued and achieved within the next decade. These include the following:

1. *In situ* high-temperature solid–gas reactions: As temperature increases (>2000 K), the amount of solid–gas reaction (e.g., oxidation) data decreases. This data problem could be overcome by utilizing aerodynamic levitation in conjunction with laser heating by varying the levitation gas while at temperature. If performed carefully, oxidation and other solid–gas reaction data could be collected up to the melting points of UHTC and RHEA materials.
2. Low-temperature applied properties: Beyond sample preservation, cryo-EM affords as-yet untapped opportunities to study low-temperature functional materials via *in-situ* experimentation at the nanoscale and in real time. Emergent magnetic phenomena, critical for the development of quantum materials, are at the forefront of this push and will see significant progress soon.
3. Mechanical testing in coupled extreme environments: There has been much progress in high-temperature mechanical testing, but there could be even greater benefits by developing additional systems to control atmospheres/corrosive environments: new sample designs (e.g., samples with cavities inside that are filled with solar salt or hydrogen passing through a tensile sample during mechanical testing).
4. Small-scale testing: Great progress has been made over the last decade. Interactions with the tip materials in nanoindentation still represent the biggest challenge due to reactions with the sample at high temperature.
5. High-resolution characterization methods of high-temperature salt corrosion: Part of the technical challenge for *in-situ* TEM studies will undoubtedly be precise control of salt chemistry and its impurities, which are known to exacerbate or totally change the nature of the salt corrosion.[228] In comparison with thermal or mechanical extremes, much more work is needed to develop comparable high-resolution characterization methods of high-temperature salt corrosion.
6. Low temperatures and light elements: Cryo-APT sample preparation and environmental transfer have made critical inroads to probing hydrogen-assisted processes at the nanoscale. These methods must be further extended to directly correlate with mechanical testing to establish interdependencies.

If these tools and techniques are added to humankind's repertoire, we could come a step closer to achieving our goals of exploring the universe, harnessing, and storing vast amounts of energy, all at a reasonable speed.

Acknowledgments

D.K.S. acknowledges support from the US Department of Energy (DOE), Office of Science, Basic Energy Sciences Materials Science and Engineering Division in developing this manuscript. The Pacific Northwest National Laboratory is a multiprogram national laboratory operated by Battelle for the US DOE under Contract No. DE-AC05-79RL01830. S.J.M. acknowledges support from the National Science Foundation (NSF), Division of Materials Research (DMR), Ceramic (CER) program under Grant No. DMR 2047084.

Author contributions

All authors contributed equally to the production of this article.

Data availability

Not applicable (this is a review; all data have been sufficiently cited).

Conflict of interest

On behalf of all authors, the corresponding author states that there is no conflict of interest.

Ethics approval and consent to participate

Not applicable.

Consent for publication

Not applicable.

References

1. D.E. Glass, "Ceramic Matrix Composite (CMC) Thermal Protection Systems (TPS) and Hot Structures for Hypersonic Vehicles," in *15th AIAA Space Planes and Hypersonic Systems and Technologies Conference* (2008), AIAA-2008-2682
2. Memorandum on the National Strategy for Space Nuclear Power and Propulsion (Space Policy Directive-6, The White House, 2021). https://trumpwhitehouse.archives.gov/presidential-actions/memorandum-national-strategy-space-nuclear-power-propulsion-space-policy-directive-6/
3. National Academies of Sciences, Engineering, and Medicine, *Space Nuclear Propulsion for Human Mars Exploration* (National Academies Press, Washington, DC, 2021). https://doi.org/10.17226/25977
4. FACT SHEET: Developing a Bold Vision for Commercial Fusion Energy (The White House, 2022). https://www.whitehouse.gov/ostp/news-updates/2022/03/15/fact-sheet-developing-a-bold-vision-for-commercial-fusion-energy/

5. European Commission, *EU Solar Energy Strategy* (2022)
6. B. Dyatkin, *MRS Bull.* **46**(3), 201 (2021)
7. M.T. Islam, N. Huda, A.B. Abdullah, R. Saidur, *Renew. Sustain. Energy Rev.* **91**, 987 (2018)
8. J. Serp, M. Allibert, O. Beneš, S. Delpech, O. Feynberg, V. Ghetta, D. Heuer, D. Holcomb, V. Ignatiev, J.L. Kloosterman, L. Luzzi, E. Merle-Lucotte, J. Uhlíř, R. Yoshioka, D. Zhimin, *Prog. Nucl. Energy* **77**, 308 (2014)
9. D. Chapin, S. Kiffer, J. Nestell, *The Very High Temperature Reactor: A Technical Summary* (2004)
10. J.A. Wright, J. Sebastian, Secondary-hardening gear steel, US Patent 8801872B2 (2008)
11. H.-J. Jou, Lower-cost, ultra-high-strength, high-toughness steel, US Patent 20160376686 (2009)
12. V. Bojarevics, K. Pericleous, *ISIJ Int.* **43**, 890 (2003)
13. J. Etay, P. Schetelat, B. Bardet, J. Priede, V. Bojarevics, K. Pericleous, *High Temp. Mater. Process.* **27**, 439 (2008)
14. W.-K. Rhim, S.K. Chung, D. Barber, K.F. Man, G. Gutt, A. Rulison, R.E. Spjut, *Rev. Sci. Instrum.* **64**, 2961 (1993)
15. W.-K. Rhim, K. Ohsaka, P.-F. Paradis, R.E. Spjut, *Rev. Sci. Instrum.* **70**, 2796 (1999)
16. P.-F. Paradis, T. Ishikawa, *Jpn. J. Appl. Phys.* **44**, 5082 (2005)
17. P.-F. Paradis, T. Ishikawa, Y. Saita, S. Yoda, *Jpn. J. Appl. Phys.* **43**, 1496 (2004)
18. H. Tamaru, C. Koyama, H. Saruwatari, Y. Nakamura, T. Ishikawa, T. Takada, *Microgravity Sci. Technol.* **30**, 643 (2018)
19. B. Glorieux, F. Millot, J.-C. Rifflet, J.-P. Coutures, *Int. J. Thermophys.* **20**, 1085 (1999)
20. C.J. Benmore, J.K.R. Weber, *Adv. Phys. X* **2**, 717 (2017)
21. D. Langstaff, M. Gunn, G.N. Greaves, A. Marsing, F. Kargl, *Rev. Sci. Instrum.* **84**, 124901 (2013)
22. Materials Development, Inc., MDI Instruments for Innovation (n.d.). https://www.matsdev.com/
23. J.K.R. Weber, D.S. Hampton, D.R. Merkley, C.A. Rey, M.M. Zatarski, P.C. Nordine, *Rev. Sci. Instrum.* **65**(2), 456 (1994)
24. P.C. Nordine, D. Merkley, J. Sickel, S. Finkelman, R. Telle, A. Kaiser, R. Prieler, *Rev. Sci. Instrum.* **83**(12), 125107 (2012)
25. E. Trinh, P. Marston, J. Robey, *J. Colloid Interface Sci.* **124**, 95 (1988)
26. Y. Bayazitoglu, G.F. Mitchell, *J. Thermophys. Heat Transf.* **9**, 694 (1995)
27. J.K.R. Weber, A. Tamalonis, C.J. Benmore, O.L.G. Alderman, S. Sendelbach, A. Hebden, M.A. Williamson, *Rev. Sci. Instrum.* **87**(7), (2016)
28. S.J. McCormack, A. Tamalonis, R.J.K. Weber, W.M. Kriven, *Rev. Sci. Instrum.* **90**, 015109 (2019)
29. T. Ishikawa, Y. Ito, J.T. Okada, P.-F. Paradis, Y. Watanabe, T. Masaki, *Meas. Sci. Technol.* **23**(12), 125602 (2012)
30. S.J. McCormack, K.-P. Tseng, R.J.K. Weber, D. Kapush, S.V. Ushakov, A. Navrotsky, W.M. Kriven, *J. Am. Ceram. Soc.* **102**(8), 4848 (2019). https://doi.org/10.1111/jace.16271
31. S.J. McCormack, K.-P. Tseng, R.J.K. Weber, D. Kapush, S.V. Ushakov, A. Navrotsky, W.M. Kriven, *J. Am. Ceram. Soc.* **102**(11), 7028 (2019)
32. C. Agca, J.C. Neuefeind, J.W. McMurray, R. Weber, A. Navrotsky, *J. Am. Ceram. Soc.* **103**(9), 4867 (2020)
33. D.L. Price, *High-Temperature Levitated Materials* (Cambridge University Press, Cambridge, 2010)
34. S.V. Ushakov, S. Hayun, W. Gong, A. Navrotsky, *Materials* (Basel) **13**, 3141 (2020)
35. R.A. Hein, P.N. Flagella, J.B. Conway, *J. Am. Ceram. Soc.* **51**, 291 (1968)
36. P. Richet, Y. Bottinga, L. Denielou, J.P. Petitet, C. Tequi, *Geochim. Cosmochim. Acta* **46**, 2639 (1982)
37. S.V. Ushakov, A. Shvarev, T. Alexeev, D. Kapush, A. Navrotsky, *J. Am. Ceram. Soc.* **100**, 754 (2017)
38. M. Fyhrie, Q.-J. Hong, D. Kapush, S.V. Ushakov, H. Liu, A. van de Walle, A. Navrotsky, *J. Chem. Thermodyn.* **132**, 405 (2019)
39. Q.-J. Hong, S.V. Ushakov, D. Kapush, C.J. Benmore, R.J.K. Weber, A. van de Walle, A. Navrotsky, *Sci. Rep.* **8**, 14962 (2018)
40. R.C. Bradshaw, D.P. Schmidt, J.R. Rogers, K.F. Kelton, R.W. Hyers, *Rev. Sci. Instrum.* **76**, 125108 (2005)
41. M. Watanabe, M. Adachi, T. Morishita, K. Higuchi, H. Kobatake, H. Fukuyama, *Faraday Discuss.* **136**, 279 (2007)
42. K. Ohsaka, S.K. Chung, W.K. Rhim, J.C. Holzer, *Appl. Phys. Lett.* **70**, 423 (1997)
43. Z. Zhou, S. Mukherjee, W.-K. Rhim, *J. Cryst. Growth* **257**, 350 (2003)
44. S. Jeon, S. Ganorkar, Y.C. Cho, J. Lee, M. Kim, J. Lee, G.W. Lee, *Metrologia* **49**(4), 045008 (2022)
45. T. Ishikawa, C. Koyama, P.-F. Paradis, J.T. Okada, Y. Nakata, Y. Watanabe, *Int. J. Refract. Metals Hard Mater.* **92**, 105305 (2020)
46. S.V. Ushakov, J. Niessen, D.G. Quirinale, R. Prieler, A. Navrotsky, R. Telle, *Materials* (Basel) **14**, 822 (2021)
47. T. Kondo, H. Muta, K. Kurosaki, F. Kargl, A. Yamaji, M. Furuya, Y. Ohishi, *Heliyon* **5**, e02049 (2019)
48. T. Ishikawa, P.-F. Paradis, J.T. Okada, Y. Watanabe, *Meas. Sci. Technol.* **23**, 025305 (2012)
49. T. Ishikawa, P.-F. Paradis, T. Itami, S. Yoda, *Meas. Sci. Technol.* **16**, 443 (2005)
50. M. Watanabe, Y. Watanabe, C. Koyama, T. Ishikawa, S. Imaizumi, M. Adachi, M. Ohtsuka, A. Chiba, Y. Koizumi, H. Fukuyama, *Thermochim. Acta* **710**, 179183 (2022)
51. S. Hakamada, A. Nakamura, M. Watanabe, F. Kargl, *Int. J. Microgravity Sci. Appl.* **34**, 340403 (2017)
52. D. Siafakas, T. Matsushita, S. Hakamada, K. Onodera, F. Kargl, A.E.W. Jarfors, M. Watanabe, *Int. J. Microgravity Sci. Appl.* **35**, 350204 (2018)
53. R. Telle, F. Greffrath, R. Prieler, *J. Eur. Ceram. Soc.* **35**, 3995 (2015)
54. L. Hennet, D. Thiaudière, C. Landron, P. Melin, D.L. Price, J.-P. Coutures, J.-F. Bérar, M.-L. Saboungi, *Appl. Phys. Lett.* **83**, 3305 (2003)
55. L.B. Skinner, C.J. Benmore, J.K.R. Weber, M.A. Williamson, A. Tamalonis, A. Hebden, T. Wiencek, O.L.G. Alderman, M. Guthrie, L. Leibowitz, J.B. Parise, *Science* **346**, 984 (2014)
56. O.L.G. Alderman, C.J. Benmore, J.K.R. Weber, L.B. Skinner, A.J. Tamalonis, S. Sendelbach, A. Hebden, M.A. Williamson, *Sci. Rep.* **8**, 2434 (2018)
57. T. Tobase, A. Yoshiasa, H. Arima, K. Sugiyama, O. Ohtaka, T. Nakatani, K. Funakoshi, S. Kohara, *Phys. Status Solidi* **255**, 1800090 (2018)
58. H. Li, Y. Yu, B. Fang, P. Xiao, S. Wang, *J. Eur. Ceram. Soc.* **42**, 4651 (2022)
59. S.J. McCormack, R.J. Weber, W.M. Kriven, *Acta Mater.* **161**, 127 (2018)
60. S.J. McCormack, W.M. Kriven, *Acta Crystallogr. Sect. B.* **75**, 227 (2019)
61. S.V. Ushakov, A. Navrotsky, R.J.K. Weber, J.C. Neuefeind, *J. Am. Ceram. Soc.* **98**, 3381 (2015)
62. S.J. McCormack, W.A. Wheeler, B.S. Hulbert, W.M. Kriven, *Acta Mater.* **200**, 187 (2020)
63. G. Jacobs, I. Egry, K. Maier, D. Platzek, J. Reske, R. Frahm, *Rev. Sci. Instrum.* **67**, 3683 (1996)
64. C. Landron, L. Hennet, J.P. Coutures, M. Gailhanou, M. Gramond, J.F. Berar, *Europhys. Lett.* **44**, 429 (1998)
65. G.N. Greaves, M.C. Wilding, S. Fearn, D. Langstaff, F. Kargl, S. Cox, Q.V. Van, O. Majérus, C.J. Benmore, R. Weber, C.M. Martin, L. Hennet, *Science* **322**, 566 (2008)
66. A.C. Barnes, L.B. Skinner, P.S. Salmon, A. Bytchkov, I. Pozdnyakova, T.O. Farmer, H.E. Fischer, *Phys. Rev. Lett.* **103**, 225702 (2009)
67. J. Kieffer, *Science* **299**, 1998 (2003)
68. H. Sinn, B. Glorieux, L. Hennet, A. Alatas, E.E. Alp, F.J. Bermejo, D.L. Price, M.-L. Saboungi, *Science* **299**, 2047 (2003)
69. I. Pozdnyakova, L. Hennet, J.-F. Brun, D. Zanghi, S. Brassamin, V. Cristiglio, D.L. Price, F. Albergamo, A. Bytchkov, S. Jahn, M.-L. Saboungi, *J. Chem. Phys.* **126**, 114505 (2007)
70. H.E. Fischer, L. Hennet, V. Cristiglio, D. Zanghi, I. Pozdnyakova, R.P. May, D.L. Price, S. Wood, *J. Phys. Condens. Matter* **19**, 415106 (2007)
71. A. Meyer, H. Schober, D.B. Dingwell, *Europhys. Lett.* **59**, 708 (2002)
72. A. Meyer, S. Stüber, D. Holland-Moritz, O. Heinen, T. Unruh, *Phys. Rev. B* **77**, 092201 (2008)
73. B. Coté, D. Massiot, F. Taulelle, J.-P. Coutures, *Chem. Geol.* **96**, 367 (1992)
74. B.T. Poe, P.F. McMillan, B. Coté, D. Massiot, J.P. Coutures, *Science* **259**, 786 (1993)
75. D. Massiot, D. Trumeau, B. Touzo, I. Farnan, J.-C. Rifflet, A. Douy, J.-P. Coutures, *J. Phys. Chem.* **99**(44), 16455 (1995)
76. P. Florian, D. Massiot, B. Poe, I. Farnan, J.-P. Coutures, *Solid State Nucl. Magn. Reson.* **5**, 233 (1995)
77. S. Boucher, J. Piwowarczyk, R.F. Marzke, B. Takulapalli, G.H. Wolf, P.F. McMillan, W.T. Petuskey, *J. Eur. Ceram. Soc.* **25**(8), 1333 (2005)
78. R.L. Grosso, E.N.S. Muccillo, D.N.F. Muche, G.S. Jawaharram, C.M. Barr, A.M. Monterrosa, R.H.R. Castro, K. Hattar, S.J. Dillon, *Nano Lett.* **20**(2), 1041 (2020)
79. H. Liu, T.E. Gage, P. Singh, A. Jaiswal, R.D. Schaller, J. Tang, S.T. Park, S.K. Gray, I. Arslan, *Nano Lett.* **21**(13), 5842 (2021)
80. T. LaGrange, M. Armstrong, K. Boyden, C.G. Brown, G.H. Campbell, J.D. Colvin, W.J. DeHope, A.M. Frank, D.J. Gibson, F.V. Hartemann, J.S. Kim, W.E. King, B.J. Pyke, B.W. Reed, M.D. Shirk, R.M. Shuttlesworth, B.C. Stuart, B.R. Torralva, N.D. Browning, *Appl. Phys. Lett.* **89**, 044105 (2006)
81. J.D. Roehling, D.R. Coughlin, J.W. Gibbs, J.K. Baldwin, J.C.E. Mertens, G.H. Campbell, A.J. Clarke, J.T. McKeown, *Acta Mater.* **131**, 22 (2017)
82. T. LaGrange, G.H. Campbell, B.W. Reed, M. Taheri, J.B. Pesavento, J.S. Kim, N.D. Browning, *Ultramicroscopy* **108**, 1441 (2008)
83. J.C. Idrobo, A.R. Lupini, T. Feng, R.R. Unocic, F.S. Walden, D.S. Gardiner, T.C. Lovejoy, N. Dellby, S.T. Pantelides, O.L. Krivanek, *Phys. Rev. Lett.* **120**, 095901 (2018)
84. A.V. Shevthenko, L.M. Lopato, *Thermochim. Acta* **93**, 537 (1985)
85. S.V. Ushakov, A. Navrotsky, *J. Am. Ceram. Soc.* **95**, 1463 (2012)
86. M.J. Vold, *Anal. Chem.* **21**, 683 (1949)
87. D. Edwards, *Methods for Phase Diagram Determination* (Elsevier, Amsterdam, 2007)
88. S.L. Boersma, *J. Am. Ceram. Soc.* **38**, 281 (1955)
89. S.V. Ushakov, A. Navrotsky, *J. Mater. Res.* **26**, 845 (2011)
90. A. Navrotsky, *J. Am. Ceram. Soc.* **97**, 3349 (2014)
91. X. Guo, J.T. White, A.T. Nelson, A. Migdisov, R. Roback, H. Xu, *J. Nucl. Mater.* **507**, 44 (2018)
92. A.A. Voskanyan, K. Lilova, S.J. McCormack, W.M. Kriven, A. Navrotsky, *Scr. Mater.* **204**, 114139 (2021)
93. T.A. Lee, A. Navrotsky, I. Molodetsky, *J. Mater. Res.* **18**, 908 (2003)

94. T.A. Lee, A. Navrotsky, *J. Mater. Res.* **19**, 1855 (2004)
95. P.K. Davies, A. Navrotsky, *J. Solid State Chem.* **38**, 264 (1981)
96. M.W. Pitcher, S.V. Ushakov, A. Navrotsky, B.F. Woodfield, G. Li, J. Boerio-Goates, B.M. Tissue, *J. Am. Ceram. Soc.* **88**(1), 160 (2004)
97. A.A. Levchenko, G. Li, J. Boerio-Goates, B.F. Woodfield, A. Navrotsky, *Chem Mater.* **18**, 6324 (2006). https://doi.org/10.1021/CM061183C
98. G. Sharma, S.V. Ushakov, A. Navrotsky, *J. Am. Ceram. Soc.* **101**, 31 (2018)
99. A.V. Radha, O. Bomati-Miguel, S.V. Ushakov, A. Navrotsky, P. Tartaj, *J. Am. Ceram. Soc.* **92**, 133 (2009)
100. J.L. Holm, O. Kleppa, *J. Inorg. Chem.* **6**, 645 (1967)
101. A. Navrotsky, *Phys. Chem. Miner.* **2**, 89 (1977)
102. A. Navrotsky, O. Kleppa, *J. Inorg. Chem.* **6**, 2119 (1967)
103. J.M. McHale, A. Navrotsky, G.R. Kowach, F.J. DiSalvo, *Chem. Eur. J.* **2**(12), 1514 (1996)
104. J.M. McHale, A. Navrotsky, F.J. DiSalvo, *Chem. Mater.* **11**, 1148 (1999). https://doi.org/10.1021/CM981096N
105. Y. Zhang, A. Navrotsky, T. Sekine, *J. Mater. Res.* **21**, 41 (2006)
106. R.M. Morcos, A. Navrotsky, T. Varga, D. Ahn, A. Saha, F. Poli, K. Müller, R. Raj, *J. Am. Ceram. Soc.* **91**(7), 2391 (2008)
107. S. Sen, S.J. Widgeon, A. Navrotsky, G. Mera, A. Tavakoli, E. Ionescu, R. Riedel, *Proc. Natl. Acad. Sci. U.S.A.* **110**(40), 15904 (2013)
108. D.A. Wigley, *Cryogenics* **8**(1), 3 (1968)
109. E. Tyukalova, J.V. Vas, R. Ignatans, A.D. Mueller, R. Medwal, M. Imamura, H. Asada, Y. Fukuma, R.S. Rawat, V. Tileli, M. Duchamp, *Acc. Chem. Res.* **54**(16), 3125 (2021)
110. Q. Shi, C.L. Snow, J. Boerio-Goates, B.F. Woodfield, *J. Chem. Thermodyn.* **42**, 1107 (2010)
111. Q. Shi, J. Boerio-Goates, B.F. Woodfield, *J. Chem. Thermodyn.* **43**, 1263 (2011)
112. M.S. Dickson, J.J. Calvin, P.F. Rosen, B.F. Woodfield, *J. Chem. Thermodyn.* **136**, 170 (2019)
113. Y. Li, W. Huang, Y. Li, W. Chiu, Y. Cui, *ACS Nano* **14**, 9263 (2020)
114. B. Gault, A. Chiaramonti, O. Cojocaru-Mirédin, P. Stender, R. Dubosq, C. Freysoldt, S.K. Makineni, T. Li, M. Moody, J.M. Cairney, *Nat. Rev. Methods Primers* **1**, 51 (2021)
115. A. Devaraj, D.E. Perea, J. Liu, L.M. Gordon, T.J. Prosa, P. Parikh, D.R. Diercks, S. Meher, R.P. Kolli, Y.S. Meng, S. Thevuthasan, *Int. Mater. Rev.* **63**(2), 68 (2018)
116. A. Navrotsky, M. Dorogova, F. Hellman, D.W. Cooke, B.L. Zink, C.E. Lesher, J. Boerio-Goates, B.F. Woodfield, B. Lang, *Proc. Natl. Acad. Sci. U.S.A.* **104**, 9187 (2007)
117. S.J. McCormack, A. Navrotsky, *Acta Mater.* **202**, 1 (2021)
118. C.M. Rost, E. Sachet, T. Borman, A. Moballegh, E.C. Dickey, D. Hou, J.L. Jones, S. Curtarolo, J.-P. Maria, *Nat. Commun.* **6**, 8485 (2015)
119. D.B. Miracle, O.N. Senkov, *Acta Mater.* **122**, 448 (2017)
120. M. Adrian, J. Dubochet, J. Lepault, A.W. McDowall, *Nature* **308**, 32 (1984)
121. M. Khoshouei, M. Radjainia, W. Baumeister, R. Danev, *Nat. Commun.* **8**, 1699 (2017)
122. J. Dubochet, J. Frank, R. Henderson, *The Development of Cryo-Electron Microscopy* (2017)
123. Y. Li, Y. Li, A. Pei, K. Yan, Y. Sun, C.-L. Wu, L.-M. Joubert, R. Chin, A.L. Koh, Y. Yu, J. Perrino, B. Butz, S. Chu, Y. Cui, *Science* **358**, 506 (2017)
124. X. Wang, Y. Li, Y.S. Meng, *Joule* **2**, 2225 (2018)
125. A.H. Mir, A. Jan. J.-M. Delaye, S. Donnelly, J. Hinks, S. Gin, *NPJ Mater. Degrad.* **4**, 11 (2020)
126. J.A. Soltis, C.M. Wallace, R.L. Penn, P.C. Burns, *J. Am. Chem. Soc.* **138**, 191 (2016)
127. J.L. Hart, J.J. Cha, *Nano Lett.* **21**, 5449 (2021)
128. D.K. Schreiber, D.E. Perea, J.V. Ryan, J.E. Evans, J.D. Vienna, *Ultramicroscopy* **194**, 89 (2018)
129. A.A. El-Zoka, S.H. Kim, S. Deville, R.C. Newman, L.T. Stephenson, B. Gault, *Sci. Adv.* **6**(49), eabd6324 (2020)
130. D.E. Perea, D.K. Schreiber, J.V. Ryan, M.G. Wirth, L. Deng, X. Lu, J. Du, J.D. Vienna, *NPJ Mater. Degrad.* **4**, 8 (2020)
131. J. Takahashi, K. Kawakami, Y. Kobayashi, T. Tarui, *Scr. Mater.* **63**, 261 (2010)
132. Y.-S. Chen, H. Lu, J. Liang, A. Rosenthal, H. Liu, G. Sneddon, I. McCarroll, Z. Zhao, W. Li, A. Guo, J.M. Cairney, *Science* **367**(6474), 171 (2020)
133. E.A. Marquis, B. Gault, *J. Appl. Phys.* **104**, 084914 (2008)
134. S. Dumpala, S.R. Broderick, P.A.J. Bagot, K. Rajan, *Ultramicroscopy* **141**, 16 (2014)
135. S.V. Lambeets, E.J. Kautz, M.G. Wirth, G.J. Orren, A. Devaraj, D.E. Perea, *Top. Catal.* **63**, 1606 (2020)
136. A.K. Nayak, V. Kumar, T. Ma, P. Werner, E. Pippel, R. Sahoo, F. Damay, U.K. Rößler, C. Felser, S.S.P. Parkin, *Nature* **548**(7669), 561 (2017)
137. C. Zhang, K.L. Firestein, J.F.S. Fernando, D. Sirwardena, J.E. von Treifeldt, D. Golberg, *Adv. Mater.* **32**(18), 1904094 (2020)
138. L. Zhang, B.K. Miller, P.A. Crozier, *Nano Lett.* **13**, 679 (2013)
139. R. Völkl, B. Fischer, *Exp. Mech.* **44**, 121 (2004)
140. B. Fischer, S. Vorberg, R. Völkl, M. Beschliesser, A. Hoffmann, *Int. J. Refract. Metals Hard Mater.* **24**(4), 292 (2006)
141. E.W. Neuman, G.E. Hilmas, W.G. Fahrenholtz, *J. Am. Ceram. Soc.* **96**, 47 (2013)
142. E.W. Neuman, G.E. Hilmas, W.G. Fahrenholtz, *J. Am. Ceram. Soc.* **99**, 597 (2016)
143. L. Feng, W. Chen, W.G. Fahrenholtz, G.E. Hilmas, *J. Am. Ceram. Soc.* **104**, 419 (2021)
144. E. Neuman, H.J. Brown-Shaklee, J.L. Watts, G.E. Hilmas, W.G. Fahrenholtz, *Am. Ceram. Soc. Bull.* **93**, 36 (2013)
145. X. Cheng, Z. Qu, R. He, S. Ai, R. Zhang, Y. Pei, D. Fang, *Rev. Sci. Instrum.* **87**(4), 045108 (2016)
146. L. Yu, F. Ren, X. Zhang, B. Pan, *Rev. Sci. Instrum.* **93**, 045106 (2022)
147. A. Haboub, H.A. Bale, J.R. Nasiatka, B.N. Cox, D.B. Marshall, R.O. Ritchie, A.A. MacDowell, *Rev. Sci. Instrum.* **85**, 083702 (2014)
148. A.A. MacDowell, H. Barnard, D.Y. Parkinson, A. Haboub, N. Larson, F. Zok, F. Panerai, N.N. Mansour, H. Bale, B. Gludovatz, C. Acevedo, D. Liu, R.O. Ritchie, "High Temperature X-Ray Micro-tomography," *AIP Conf. Proc.* **1741**, 050005 (2016)
149. P.R. Sreenivasan, S.K. Ray, "Mechanical Testing at High Strain Rates," in *Encyclopedia of Materials: Science and Technology*, 2nd edn. (Elsevier, 2001). https://doi.org/10.1016/B0-08-043152-6/00919-0
150. Q.B. Dou, K.R. Wu, T. Suo, C. Zhang, X. Guo, Y.Z. Guo, W.G. Guo, Y.L. Li, *Acta Mech. Sin.* **36**, 1275 (2020)
151. Y. Li, Y. Guo, H. Hu, Q. Wei, *Int. J. Impact Eng.* **36**, 177 (2009)
152. O. Umezawa, *Mater. Perform. Charact.* **10**, 20200138 (2021)
153. X. Gao, R. Chen, T. Liu, H. Fang, G. Qin, Y. Su, J. Guo, *J. Mater. Sci.* **57**(12), 6573 (2022)
154. A.S. Tirunilai, J. Sas, K.-P. Weiss, H. Chen, D.V. Szabó, S. Schlabach, S. Haas, D. Geissler, J. Freudenberger, M. Heilmaier, A. Kauffmann, *J. Mater. Res.* **33**, 3287 (2018)
155. J.M. Wheeler, D.E.J. Armstrong, W. Heinz, R. Schwaiger, *Curr. Opin. Solid State Mater. Sci.* **19**, 354 (2015)
156. A. Barnoush, P. Hosemann, J. Molina-Aldareguia, J.M. Wheeler, *MRS Bull.* **44**(6), 471 (2019)
157. I.-C. Choi, C. Brandl, R. Schwaiger, *Acta Mater.* **140**, 107 (2017)
158. C. Brandl, I.-C. Choi, R. Schwaiger, *Mater. Sci. Eng. A* **852**, 143629 (2022). https://doi.org/10.1016/J.MSEA.2022.143629
159. C. Minnert, W.C. Oliver, K. Durst, *Mater. Des.* **192**, 108727 (2020)
160. J.M. Wheeler, J. Michler, *Rev. Sci. Instrum.* **84**, 101301 (2013)
161. S.A. Syed Asif, J.B. Pethica, *J. Adhes.* **67**, 153 (1998)
162. S. Wang, H. Xu, Y. Wang, L. Kong, Z. Wang, S. Liu, J. Zhang, H. Zhao, *Rev. Sci. Instrum.* **90**(1) 015117 (2019)
163. P. Hosemann, C. Shin, D. Kiener, *J. Mater. Res.* **30**, 1231 (2015)
164. P. Hosemann, *Scr. Mater.* **143**, 161 (2018)
165. A.S. Ebner, S. Brinckmann, E. Plesiutschnig, H. Clemens, R. Pippan, V. Maier-Kiener, *JOM* **72**, 2020 (2020)
166. A. Barnoush, H. Vehoff, *Acta Mater.* **58**, 5274 (2010)
167. K. Tomatsu, K. Miyata, T. Omura, *ISIJ Int.* **56**, 418 (2016)
168. J. Kim, C.C. Tasan, *Int. J. Hydrogen Energy* **44**, 6333 (2019)
169. C. Zehnder, J.-N. Peltzer, J.S.K.-L. Gibson, S. Korte-Kerzel, *Mater. Des.* **151**, 17 (2018)
170. G. Guillonneau, M. Mieszala, J. Wehrs, J. Schwiedrzik, S. Grop, D. Frey, L. Philippe, J.-M. Breguet, J. Michler, J.M. Wheeler, *Mater. Des.* **148**, 39 (2018)
171. Z. Zhang, M.M. Mao, J. Wang, B. Gludovatz, Z. Zhang, S.X. Mao, E.P. George, Q. Yu, R.O. Ritchie, *Nat. Commun.* **6**, 10143 (2015)
172. Z. Shen, M. Meisnar, K. Arioka, S. Lozano-Perez, *Acta Mater.* **165**, 73 (2019)
173. C. Ophus, *Microsc. Microanal.* **25**, 563 (2019)
174. Q. Yu, L. Qi, K. Chen, R.K. Mishra, J. Li, A.M. Minor, *Nano Lett.* **12**(2), 887 (2012)
175. S. Li, C.A. Powell, S. Mathaudhu, B. Gwalani, A. Devaraj, C. Wang, *J. Mater. Sci.* **57**, 12177 (2022)
176. J. Liu, R. Niu, J. Gu, M. Cabral, M. Song, X. Liao, *Sci. Rep.* **10**, 10324 (2020)
177. S.R. Spurgeon, C. Ophus, L. Jones, A. Petford-Long, S.V. Kalinin, M.J. Olszta, R.E. Dunin-Borkowski, N. Salmon, K. Hattar, W.-C.D. Yang, R. Sharma, Y. Du, A. Chiaramonti, H. Zheng, E.C. Buck, L. Kovarik, R.L. Penn, D. Li, X. Zhang, M. Murayama, M.L. Taheri, *Nat. Mater.* **20**, 274 (2021)
178. K. Vignarooban, X. Xu, K. Wang, E.E. Molina, P. Li, D. Gervasio, A.M. Kannan, *Appl. Energy* **159**, 206 (2015)
179. M. Walczak, F. Pineda, Á.G. Fernández, C. Mata-Torres, R.A. Escobar, *Renew. Sustain. Energy Rev.* **86**, 22 (2018)
180. M. Sarvghad, S. Delkasar Maher, D. Collard, M. Tassan, G. Will, T.A. Steinberg, *Energy Storage Mater.* **14**, 179 (2018)
181. A. Bonk, S. Sau, N. Uranga, M. Hernaiz, T. Bauer, *Prog. Energy Combust. Sci.* **67**, 69 (2018)
182. K. Vignarooban, X. Xu, A. Arvay, K. Hsu, A.M. Kannan, *Appl. Energy* **146**, 383 (2015)
183. Y. Li, X. Xu, X. Wang, P. Li, Q. Hao, B. Xiao, *Sol. Energy* **152**, 57 (2017)
184. W. Ding, H. Shi, Y. Xiu, A. Bonk, A. Weisenburger, A. Jianu, T. Bauer, *Sol. Energy Mater. Sol. Cells* **184**, 22 (2018)

185. W. Ding, H. Shi, A. Jianu, Y. Xiu, A. Bonk, A. Weisenburger, T. Bauer, *Sol. Energy Mater. Sol. Cells* **193**, 298 (2019)
186. B. Grégoire, C. Oskay, T.M. Meißner, M.C. Galetz, *Sol. Energy Mater. Sol. Cells* **215**, 110659 (2020)
187. B. Grégoire, C. Oskay, T.M. Meißner, M.C. Galetz, *Sol. Energy Mater. Sol. Cells* **216**, 110675 (2020)
188. F. Sutter, C. Oskay, M. Galetz, T.C. Diamantino, F. Pedrosa, I. Figueira, S. Glumm, A. Bonk, A. Agüero, S. Rodriguez Catela, T.J. Reche-Navarro, S. Caron, *Sol. Energy Mater. Sol. Cells* **232**(3), 111331 (2021)
189. X. Li, L. Chang, C. Liu, B. Leng, X. Ye, F. Han, X. Yang, *Corros. Sci.* **191**, 109784 (2021)
190. S.S. Raiman, J.M. Kurley, D. Sulejmanovic, A. Willoughby, S. Nelson, K. Mao, C.M. Parish, M.S. Greenwood, B.A. Pint, *J. Nucl. Mater.* **561**, 153551 (2022)
191. H. Atmani, J.J. Rameau, *Corros. Sci.* **24**, 279 (1984)
192. G. Zheng, B. Kelleher, G. Cao, M. Anderson, T. Allen, K. Sridharan, *J. Nucl. Mater.* **461**, 143 (2015)
193. H. Li, X. Yang, X. Yin, J. Tang, J. Gong, C. Fuyang, *Mater. Corros.* **71**(6), 938 (2020)
194. A. Mallco, F. Pineda, M. Mendoza, M. Henriquez, C. Carrasco, V. Vergara, E. Fuentealba, A.G. Fernandez, *Sol. Energy Mater. Sol. Cells* **238**, 111623 (2022)
195. K. Beierschmitt, M. Buchanan, A. Clark, I. Robertson, P. Britt, A. Navrotsky, P. Burns, P. Tortorelli, A. Misra, J. Wishart, P. Fenter, A. Gewirth, B. Wirth, B. Mincher, I. Szlufarska, J. Busby, L. Horton, B. Garrett, J. Vetrano, P. Wilk, K. Runkles, S. Kung, S. Lesica, B. Wyatt, D. Counce, K. Jones, *Basic Research Needs for Future Nuclear Energy: Report of the Basic Energy Sciences Workshop for Future Nuclear Energy, August 9–11, 2017* (US Department of Energy, Office of Scientific and Technical Information, 2017). https://doi.org/10.2172/1616270
196. P.L. Andresen, G.S. Was, *J. Nucl. Mater.* **517**, 380 (2019)
197. X. Liu, A. Ronne, L.-C. Yu, Y. Liu, M. Ge, C.-H. Lin, B. Layne, P. Halstenberg, D.S. Maltsev, A.S. Ivanov, S. Antonelli, S. Dai, W.-K. Lee, S.M. Mahurin, A.I. Frenkel, J.F. Wishart, X. Xiao, Y.-K. Chen-Wiegart, *Nat. Commun.* **12**, 3441 (2021)
198. J. Erlebacher, M.J. Aziz, A. Karma, N. Dimitrov, K. Sieradzki, *Nature* **410**, 450 (2001)
199. K. Hattar, R.R. Unocic, *Recent Developments in Analytical Techniques for Corrosion Research* (Springer, Berlin, 2022). https://doi.org/10.1007/978-3-030-89101-5_6
200. K. Bawane, X. Liu, R. Gakhar, M. Woods, M. Ge, X. Xiao, W.-K. Lee, P. Halstenberg, S. Dai, S. Mahurin, S.M. Pimblott, J.F. Wishart, Y.K. Chen-Wiegart, L. He, *Corros. Sci.* **195**, 109962 (2022)
201. W.G. Fahrenholtz, G.E. Hilmas, *Scr. Mater.* **129**, 94 (2017)
202. E. Wichina, E. Opila, M. Opeka, W. Fahrenholtz, I. Talmy, *Electrochem. Soc. Interface* **16**(4), 30 (2007)
203. J. Justin, A. Jankowiak, *Aerospace Lab* **3** (2011)
204. B. Gorr, S. Schellert, F. Müller, H.-J. Christ, A. Kauffmann, M. Heilmaier, *Adv. Eng. Mater.* **23**(5), 2001047 (2021)
205. B. Gorr, F. Müller, S. Schellert, H.-J. Christ, H. Chen, A. Kauffmann, M. Heilmaier, *Corros. Sci.* **166**(2), (2020)
206. M. Miller-Oana, P. Neff, M. Valdez, A. Powell, M. Packard, L.S. Walker, E.L. Corral, *J. Am. Ceram. Soc.* **98**(4), 1300 (2015)
207. A. Paul, J.G.P. Binner, B. Vaidhyanathan, A.C.J. Heaton, P.M. Brown, *J. Microsc.* **250**, 122 (2013)
208. S.R.C.M. Tammana, M. Duan, J. Zou, J. Wade, V. Venkatachalam, B. Baker, S. Nayebossadri, J. Binner, *Open Ceram.* **10**, 100270 (2022)
209. P.J. Ritt, P.A. Williams, S.C. Splinter, J.H. Perepezko, *J. Eur. Ceram. Soc.* **34**, 3521 (2014)
210. E.J. Opila, *J. Am. Ceram. Soc.* **86**, 1238 (2003)
211. M. Weber, B. Gorr, H.-J. Christ, S. Obert, A. Kauffmann, M. Heilmaier, *Adv. Eng. Mater.* **22**(7), 2000219 (2020)
212. S. Joseph, P. Kontis, Y. Chang, Y. Shi, D. Raabe, B. Gault, D. Dye, *Acta Mater.* **227**, 117687 (2022)
213. M.G. Burke, G. Bertali, E. Prestat, F. Scenini, S.J. Haigh, *Ultramicroscopy* **176**, 46 (2017)
214. L. Luo, M. Su, P. Yan, L. Zou, D.K. Schreiber, D.R. Baer, Z. Zhu, G. Zhou, Y. Wang, S.M. Bruemmer, Z. Xu, C. Wang, *Nat. Mater.* **17**(6), 514 (2018)
215. F. Müller, B. Gorr, H.-J. Christ, J. Müller, B. Butz, H. Chen, A. Kauffmann, M. Heilmaier, *Corros. Sci.* **159**, 108161 (2019)
216. B. Song, Y. Yang, M. Rabbani, T.T. Yang, K. He, X. Hu, Y. Yuan, P. Ghildiyal, V.P. Dravid, M.R. Zachariah, W.A. Saidi, Y. Liu, R. Shahbazian-Yassar, *ACS Nano* **14**(11), 15131 (2020)
217. T. Kremic, D. Vento, N. Lalli, T. Palinski, "Extreme Environment Simulation - Current and New Capabilities to Simulate Venus and Other Planetary Bodies," in *2014 IEEE Aerospace Conference* (IEEE, Big Sky, March 1–8, 2014), pp. 1–9. https://doi.org/10.1109/AERO.2014.6836350
218. A. Santos, J. Balcerski, D.M. Burr, J. Helbert, G. Hunter, N. Izenberg, N. Johnson, E. Kohler, T. Kremic, S. Port, *Bull. Am. Astron. Soc.* **53**(4), 158 (2021)
219. D. Lukco, D.J. Spry, R.P. Harvey, G.C.C. Costa, R.S. Okojie, A. Avishai, L.M. Nakley, P.G. Neudeck, G.W. Hunter, *Earth Space Sci.* **5**(7), 270 (2018)
220. P.G. Neudeck, R.D. Meredith, L. Chen, D.J. Spry, L.M. Nakley, G.W. Hunter, *AIP Adv.* **6**(12), 125119 (2016)
221. P.G. Neudeck, L. Chen, R.D. Meredith, D. Lukco, D.J. Spry, L.M. Nakley, G.W. Hunter, *IEEE J. Electron Devices Soc.* **7**, 100 (2019)
222. L. Chen, P.G. Neudeck, R.D. Meredith, D. Lukco, D.J. Spry, L.M. Nakley, K.G. Phillips, G.M. Beheim, G.W. Hunter, "Sixty Earth-Days Test of a Prototype Pt/HTCC Alumina Package in Simulated Venus Environment," in *Additional Conferences (Device Packaging, HiTEC, HiTEN, & CICMT)* **2018**, 000015 (2018)
223. J.L. Jordan, G.E. Ponchak, "Rectangular Waveguide Resonator for Gas Permittivity Measurement at X-Band," in *2018 IEEE Topical Conference on Wireless Sensors and Sensor and Networks (WiSNet)* (IEEE, Anaheim, January 14–17, 2018), pp. 59–62. https://doi.org/10.1109/WISNET.2018.8311564
224. Z. Harutyunyan, Y. Gasparyan, S. Ryabtsev, V. Efimov, O. Ogorodnikova, A. Pisarev, S. Kanashenko, *J. Nucl. Mater.* **548**, 152848 (2021)
225. J. Takahashi, K. Kawakami, Y. Sakiyama, T. Ohmura, *Mater. Charact.* **178**, 111282 (2021)
226. Y.-S. Chen, D. Haley, S.S.A. Gerstl, A.J. London, F. Sweeney, R.A. Wepf, W.M. Rainforth, P.A.J. Bagot, M.P. Moody, *Science* **355**(6330), 1196 (2017)
227. Y.-S. Chen, M.J. Griffith, J.M. Cairney, *Nano Today* **37**, 101107 (2021)
228. K. Sridharan, T.R. Allen, "Corrosion in Molten Salts," in *Molten Salts Chemistry: From Lab to Applications*, ed. by F. Lantelme, H. Groult (Elsevier, 2013), chap. 12, pp. 241–267. https://doi.org/10.1016/B978-0-12-398538-5.00012-3

Daniel K. Schreiber is a senior materials scientist in the Nuclear Sciences Division of the Energy and Environment Directorate at the US Department of Energy Pacific Northwest National Laboratory (PNNL). He obtained his bachelor's and doctoral degrees in materials science and engineering from Michigan State University and Northwestern University, respectively. In 2011, he joined PNNL as a postdoctoral research associate, where he has remained as a senior scientist with a specialty in high-resolution microscopy and atom probe tomography. His research is focused on understanding the fundamental aspects of material degradation in extreme environments, especially high-temperature corrosion, cracking, and radiation damage in nuclear energy systems. Schreiber can be reached by email at daniel.schreiber@pnnl.gov.

Ruth Schwaiger has been director at the Institute of Energy and Climate Research (Forschungszentrum Jülich) and professor for energy engineering materials at RWTH Aachen University since 2019. She studied physics at the Technische Universität Wien in Vienna, Austria, conducted her doctoral research at the Max Planck Institute for Metals Research in Stuttgart, Germany, and obtained her doctoral degree from the University of Stuttgart, Germany, in 2002. After completing postdoctoral research at the Massachusetts Institute of Technology, Schwaiger joined the Forschungszentrum Karlsruhe in Germany in 2004, moved to a management consulting firm in 2007 before joining the Karlsruhe Institute of Technology, Germany, in 2010. Her research interests focus on the mechanical behavior of materials in extreme environments and on understanding the microstructural changes at high temperatures. Her research aims to develop a mechanism-based understanding of deformation, degradation, and failure. Schwaiger can be reached by email at r.schwaiger@fz-juelich.de.

Martin Heilmaier is the chair for materials science and engineering at the Institute for Applied Materials, Karlsruhe Institute of Technology, Germany. He graduated from the University of Erlangen-Nürnberg in 1988 and received his PhD degree from the same university in 1992. He completed postdoctoral stays at IFW Dresden and The University of Western Australia in Perth, and served as team leader R&D of refractory metals at Plansee SE, Reutte, Austria. He held full professor positions at Otto-von-Guericke-University Magdeburg (2002–2008) and at TU Darmstadt (2008–2011). His research areas include the development of novel high-temperature structural materials, intermetallic compounds, high-entropy alloys, as well as their mechanical testing under extreme environmental conditions. Heilmaier can be reached by email at martin.heilmaier@kit.edu.

Scott J. McCormack is an assistant professor of materials science and engineering at the University of California, Davis. He completed a bachelor of engineering degree, majoring in materials engineering at the University of Wollongong, Australia, in 2013. He then completed his PhD degree in materials science and engineering from the University of Illinois at Urbana-Champaign in 2019. His research interests focus on the interplay of crystallography and phase equilibria of materials in extreme environments, with an emphasis on high temperatures (above 3000°C) for applications in hypersonic platforms, nuclear fission and fusion, and space exploration. McCormack can be reached by email at sjmccormack@ucdavis.edu.